

Quantum Annealing-Infused Microgrids Formation: Distribution System Restoration and Resilience Enhancement

Nima Nikmehr¹, Senior Member, IEEE, Peng Zhang², Honghao Zheng³, Senior Member, IEEE, Tzu-Chieh Wei⁴, Gang He⁵, and Yacov A. Shamash⁶, Fellow, IEEE

Abstract—In this paper, the use of quantum computing is explored to solve a crucial optimization problem in the formation of microgrids (MGs), which can enhance the resilience of distribution networks against natural disasters or faults. The study focuses on developing a quantum-inspired optimization model for critical load restoration via MGs formation, leveraging the power of quantum annealing to solve complex combinatorial problems that classical methods struggle with. The Constrained Quadratic Model (CQM) solver from D-Wave is used to merge classical and quantum optimization approaches, delivering improved solutions to complex optimization problems. The solver has been optimized to take advantage of quantum computing’s parallelism to provide high-performance solutions. The study compares outcomes from the D-Wave hybrid quantum-classical solver and the classical Gurobi solver, underscoring the effectiveness of quantum computing in addressing resilience-oriented optimization challenges. This assessment is validated through two case studies: the IEEE 37-bus system and the IEEE 240-bus distribution system.

Index Terms—Quantum computing, load restoration, microgrids formation, quantum annealing, resilience.

I. INTRODUCTION

IN THE past four decades, the U.S. has sustained hundreds of billion-dollar weather and climate disasters causing 2.6 trillion dollar losses as well as major blackouts [1]. Given the unpredictability and high impact nature of such events, research

Manuscript received 26 August 2023; revised 7 January 2024 and 17 March 2024; accepted 3 May 2024. Date of publication 9 May 2024; date of current version 27 December 2024. This work was supported in part by the National Science Foundation under Grant ITE-2134840 and in part by the Department of Navy under Award N00014-23-1-2124 through the Office of Naval Research. Paper no. TPWRS-01331-2023. (Corresponding author: Peng Zhang.)

Nima Nikmehr is with Hitachi Energy, Albany, NY 12202 USA (e-mail: n.a.nikmehr@gmail.com).

Peng Zhang and Yacov A. Shamash are with the Department of Electrical and Computer Engineering, Stony Brook University, Stony Brook, NY 11794 USA (e-mail: p.zhang@stonybrook.edu; yacov.shamash@stonybrook.edu).

Honghao Zheng is with Midcontinent Independent System Operator, Carmel, IN 46032 USA (e-mail: hozheng@misoenergy.org).

Tzu-Chieh Wei is with the C.N. Yang Institute for Theoretical Physics, Stony Brook University, Stony Brook, NY 11794-3800 USA (e-mail: tzu-chieh.wei@stonybrook.edu).

Gang He is with the Marx School of Public and International Affairs, Baruch College, City University of New York, New York, NY 10010 USA (e-mail: gang.he@baruch.cuny.edu).

Color versions of one or more figures in this article are available at <https://doi.org/10.1109/TPWRS.2024.3399122>.

Digital Object Identifier 10.1109/TPWRS.2024.3399122

focused on enhancing the resilience of power systems against natural disasters is becoming increasingly imperative [2].

The formation of microgrids (MGs) is a potential solution to restore local loads in response to the devastating effects of natural disasters [3], [4]. In [5], the factors considered in the formation of MGs and the maximum restoration of loads include the switching status of distribution system lines, nodes, loads, and the presence of distributed generators (DGs). In [6], the approach to restore critical loads involves optimizing the distribution system reconfiguration in order to increase the service time of microgrids while considering the dynamic performance of DGs. The work in [7] evaluates the resilience of MGs by considering the continuous operating time, with the goal of minimizing voltage fluctuations and maximizing critical load restoration in the face of uncertainties from DGs and load profile. In [8], a mixed-integer linear programming (MILP) model is introduced to maximize the resilience of a distribution system in the event of a natural disaster, while simultaneously reducing the likelihood of post-restoration failures. In [9], privacy concerns for MGs are addressed by assigning an independent distribution system operator to each MG entity and further, an incentive-based demand response model is introduced to encourage MGs to participate in the load restoration effort.

Solving microgrids formation online, however, is a daunting task. Microgrids formation is an MILP problem, which results in a complex combinatorial challenge [6], [10], [11]. The complexity of forming microgrids and restoring loads is anticipated to rise due to the introduction of numerous decision variables and constraints caused by the widespread adoption of DGs. As a result, it is imperative to investigate new solution techniques that can competently tackle the complex problem.

To address the challenge of restoring critical loads using microgrids formation, various methodologies have been introduced. These studies have primarily focused on developing optimized models aimed at maximizing load restoration after a natural disaster. In [12], an optimization model based on MILP is proposed with the aim of restoring the maximum amount of critical loads. To deal with the uncertainties in load demand, the authors adopt Information Gap Decision Theory. In [13], a novel approach is proposed to restore critical loads after a fault in microgrids. A distributed multi-agent algorithm is employed, taking into account the average consensus theorem to coordinate the decisions of neighboring microgrids in

a synchronous manner. The solutions obtained are then evaluated for optimality using particle swarm optimization. In [14], the use of a mixed-integer semidefinite program is introduced to maximize the amount of critical loads restored after a natural disaster. In [15], the load restoration problem in distribution systems is formulated as a mixed-integer second-order cone program to optimize the outcome. The use of deep reinforcement learning for the microgrids formation is investigated in [16] to find near-optimal microgrid formations in distribution systems.

The optimization problem for forming MGs involves many binary and integer decision variables and can lead to combinatorial complexity, making it challenging to find the optimal solution using aforementioned classical optimization methods. With the increasing scale of the problem, these methods may struggle to find near-optimal or global solutions. To overcome these limitations, quantum computing (QC) offers a promising approach to solve combinatorial problems that contain different types of variables and many constraints. The applications of quantum computing in the power systems sector have been reviewed in [17]. The review highlights the potential of quantum computing in different areas of power systems, such as fundamental power analytics, power system operation and optimization, power system stability and control, communication security, and machine learning. As a first step towards solving one of the important operational optimization problems in power systems, [18], [19] consider the distributed unit commitment problem as an MILP optimization problem and develop a quantum model of unit commitment. They then use a quantum version of the alternating direction method of multipliers (ADMM) to solve the problem in a distributed manner by decomposing the main problem into several subproblems. This approach is promising as it does not impose limitations on the number of qubits and can solve combinatorial problems that are intractable for classical computers. In the study conducted in [20], the authors combined quantum computing and classical Surrogate Lagrangian Relaxation (SLR) to tackle large-scale combinatorial problems, such as the unit commitment problem. In this approach, the subproblems that contain binary variables are solved using Quantum Approximate Optimization Algorithm (QAOA), while the continuous subproblems are tackled by classical solvers.

Quantum computing is currently performed using either gate-based or annealing-based approaches. In gate-based quantum computers, the input qubits are put into quantum states, which then undergo changes through unitary operators and quantum gates, leading to a final state of the qubit(s) that is then measured. This process of transitioning from the input qubits to the final measurement is referred to as a quantum circuit. Currently, IBM provides commercial access to quantum computers with up to 433 qubits, while public quantum devices provide access to up to 32 qubits. IBM has set a roadmap for the development of the Condor processor, which will have 1121 qubits, by 2023 [21]. However, the current gate-based quantum computing devices face limitations in terms of the number of qubits and connectivity, making it challenging to solve large-scale problems. To address this challenge, quantum annealing approaches can be used to solve combinatorial optimization problems, such

as the Quadratic Unconstrained Binary Optimization (QUBO) problem. For instance, the D-Wave company utilizes quantum annealing (QA) to solve large-scale QUBO problems by utilizing a lattice of qubits [22]. Quantum annealing, distinct from reinforcement learning in solving load restoration problem through MGs formation [16], leverages quantum tunneling to enhance the search for optimal microgrid configurations. Its parallelism and superposition features offer a unique advantage in resilience planning against natural disasters. Moreover, the stochastic nature allows for diverse exploration, uncovering unconventional configurations that enhance resilience.

Considering the limitations of classical optimization methods and the advancements in quantum computing, the following are the key contributions of this paper:

- A QUBO model for networked MGs formation-based load restoration problem is created, which can be solved using quantum annealing. This involves constructing the Hamiltonian of Ising model as an energy function, representing the objective function and system topology and operational constraints.
- The solution to the load restoration problem using MGs formation is obtained through the use of the D-Wave quantum machine and the quantum annealing approach. The hybrid quantum-classical solver offered by D-Wave is utilized to carry out the load restoration problem, allowing the quantum processor to address non-continuous decision variables and a large number of constraints. Additionally, this solver demonstrates significantly improved efficiency in comparison to traditional classical solvers in the resolution of large scale distribution systems.

II. PROBLEM FORMULATION

In this work, the strategy for restoring a distribution system following a significant fault in the main grid is through the formation of microgrids. The objective of forming microgrids is to modify the topology of the distribution system to prioritize the restoration of the maximum number of prioritized loads through the control of line and load switches. It is important to note that the switches in our model are remotely controlled automatic switch devices. The placement of these switches at different lines and nodes provides adaptable control over the network's topology.

In the radial distribution system studied in this paper, following a natural disaster, it is the responsibility of DGs to energize the critical loads of microgrids before the main grids are restored. Additionally, each MG is supplied by one or multiple DGs. DG units are dispatchable and actively controllable and can be scheduled to optimize their real and reactive power outputs.

In the rest of this section, the MGs formation problem is modeled as an MILP to restore the maximum prioritized loads considering the operational and topological constraints.

A. MGs Formation Constraints

In the studied radial distribution system, the problem of optimally restoring the system after a natural disaster involves several constraints that must be satisfied. These constraints

include node and line-related constraints, microgrid connectivity constraints, microgrid load pick-up constraints, and operational constraints related to the distribution system and microgrids such as real and reactive power flow, voltage limits, power generation capacity of distributed generators, and balance of real and reactive power at each node.

1) *Belonging of Nodes and Lines to MGs*: This constraint states that every microgrid has lines and loads located at nodes, and that a single node cannot be part of multiple microgrids. Additionally, if two nodes are part of the same microgrid, the line connecting them must also be part of that microgrid. To establish this constraint, the nodes are first divided into active and passive nodes. Active nodes are powered by the distribution system and distributed generators, while passive nodes have been isolated from the main grid and microgrids as a result of damage caused by natural disasters and cannot be connected to the energized portion of the system. Assume a radial distribution system with B nodes. Node $i \in B$ will be removed from the node set N if it is a passive node. Therefore, after removing the passive nodes, there will be B^* nodes.

Node $i \in B^*$ should only belong to one of the microgrids in the set M . To realize the node belonging constraint, a binary decision variable w_i should be defined for node $i \in B^*$. Node i belongs to MG m if $w_{im} = 1$, otherwise $w_{im} = 0$.

$$\sum_{m \in M} w_{im} = 1, i \in B^*. \quad (1)$$

Additionally, the assignment of a line to an MG depends on the assignment of its connected nodes to that microgrid. If node $i \in B^*$ and node $\tilde{i} \in B^*$ are two nodes of MG m , the connected line $l_{i\tilde{i}}$ between nodes i and \tilde{i} belongs to the same microgrid. To model the line belonging constraint, a binary decision variable should be assigned to each line so that the following equality constraint is satisfied:

$$l_{i\tilde{i}}^m = w_{im} \cdot w_{\tilde{i}m}, \quad \forall i, \tilde{i} \in B^*, m \in M \quad (2)$$

The equality constraint (2) can be converted to the following set of inequality constraints:

$$l_{i\tilde{i}}^m \leq w_{im}, \quad \forall i, \tilde{i} \in B^*, m \in M, \quad (3a)$$

$$l_{i\tilde{i}}^m \leq w_{\tilde{i}m}, \quad \forall i, \tilde{i} \in B^*, m \in M, \quad (3b)$$

$$l_{i\tilde{i}}^m \geq w_{im} + w_{\tilde{i}m} - 1, \quad \forall i, \tilde{i} \in B^*, m \in M. \quad (3c)$$

2) *Connectivity of Nodes in Each Microgrid*: In order to ensure connectivity between nodes in an MG with B^* nodes, a parent node must be designated for each node. The nodes fed by the parent node are referred to as children nodes. To fulfill the connectivity constraint within each microgrid, a parent-child node relationship must be established. A child node can only belong to an MG if its parent belongs to the same MG. This constraint is integral in maintaining the radial structure of distribution networks, serving as a crucial element in the overall network topology. The constraint can be written as follows:

$$w_{im} \leq w_{\tilde{i}m}, \quad \forall i, \tilde{i} \in B^*, m \in M, \quad (4)$$

where, $w_{\tilde{i}m}$ is the belonging status of parent node \tilde{i} to MG m .

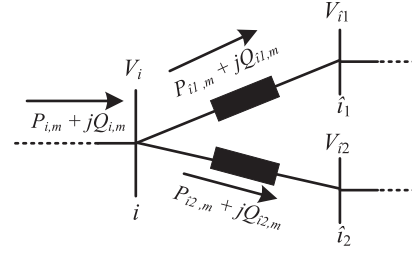


Fig. 1. Power flow model in a sample microgrid including parent and children nodes.

3) *Energized Loads Constraint*: In this constraint, each load is connected to a node. To show the status of a energized load connected to a node, the energized load status is indicated by a binary decision variable e_i . For a energized load in microgrid m , the load should be connected to node n of MG m . Therefore, the energized load status should be indicated as following:

$$e_{im} = w_{im} \cdot s_i, \quad \forall i \in B^*, m \in M, \quad (5)$$

where, s_i is a binary decision variable, which indicates the connection status of i th energized load to node $i \in B^*$ of microgrid m . If load i in microgrid m is connected to node i ($s_i = 1$) and node i belongs to MG m ($w_{im} = 1$), as a result the load is energized with the indication $e_{im} = 1$, otherwise $e_{im} = 0$. To convert the nonlinear (5) to inequality linear equations, the equation is replaced by the following constraints:

$$e_{im} \leq w_{im}, \quad \forall i \in B^*, m \in M, \quad (6a)$$

$$e_{im} \leq s_i, \quad \forall i \in B^*, m \in M, \quad (6b)$$

$$e_{im} \geq w_{im} + s_i - 1, \quad \forall i \in B^*, m \in M. \quad (6c)$$

4) *MG Operational Constraints*: The linearized DistFlow model is used for power flow constraints [23], [24]. Given the distribution network Fig. 1, the linearized DistFlow model can be written as follows [25]:

$$P_{i,m}^{flow} = \sum_{\tilde{i}} P_{i-\tilde{i},m}^{flow} + e_{i,m} \cdot P_{i,m}^L, \quad \forall i, \tilde{i} \in B^*, m \in M, \quad (7a)$$

$$Q_{i,m}^{flow} = \sum_{\tilde{i}} Q_{i-\tilde{i},m}^{flow} + e_{i,m} \cdot Q_{i,m}^L, \quad \forall i, \tilde{i} \in B^*, m \in M, \quad (7b)$$

$$V_{i,m} = V_{\tilde{i},m} - \frac{R_{i-\tilde{i}} \cdot P_{i,m}^{flow} + X_{i-\tilde{i}} \cdot Q_{i,m}^{flow}}{V_{0,m}}, \quad \forall i, \tilde{i} \in B^*, \quad (7c)$$

where, $P_{i,m}^{flow}$ and $Q_{i,m}^{flow}$ are real and reactive power in-flow at node i of MG m , respectively. Real and reactive powers $P_{i-\tilde{i},m}^{flow}$ and $Q_{i-\tilde{i},m}^{flow}$ represent the injected real and reactive power to children nodes \tilde{i} from node i in microgrid m , respectively. Moreover, $P_{i,m}^L$ and $Q_{i,m}^L$ are real and reactive loads, respectively. While the voltage at node i is denoted by V_i , $V_{0,m}$ describes the reference voltage at DG node in MG m . The resistance and reactance of distribution lines $i - \tilde{i}$ are described by $R_{i-\tilde{i}}$ and $X_{i-\tilde{i}}$, respectively.

The in-flow real and reactive powers and nodes voltage are within a range:

$$0 \leq P_{i,m}^{flow} \leq w_{im} \cdot \bar{P}_{DG,m}, \quad \forall i \in B^*, m \in M, \quad (8a)$$

$$0 \leq Q_{i,m}^{flow} \leq w_{im} \cdot \bar{Q}_{DG,m}, \quad \forall i \in B^*, m \in M, \quad (8b)$$

$$0 \leq V_{i,m} \leq w_{im} \cdot V_{0,m}, \quad \forall i \in B^*, m \in M, \quad (8c)$$

where, $\bar{P}_{DG,m}$ and $\bar{Q}_{DG,m}$ are maximum value of produced real and reactive powers by the DG located at MG m .

B. Microgrids Formation Objective Function

The goal of the optimization problem is to maximize the restoration of prioritized loads after a disaster. Loads are assigned different weights based on their priority, with higher priority loads receiving a larger weight. The weighted load restoration objective function is written as follows:

$$\max_{w,l,s,e,P_{flow},Q_{flow},V} \sum_{i \in B^*} \sum_{m \in M} c_i \cdot e_{im} \cdot P_{i,m}^L \quad (9)$$

where, c_i is the priority weight of load at node i .

III. QUANTUM-AMENABLE RESILIENT MICROGRIDS FORMATION

In this section, an overview of quantum computing is presented, followed by the development of a quantum-based model for the formation of resilient microgrids.

In this section, we develop a comprehensive Ising model encompassing all power system components, along with formulating the objective function and constraints' Hamiltonian. The inherent flexibility of our developed model allows for seamless integration of diverse constraints.

A. Background of Quantum Computing

To grasp the fundamentals of quantum computing and its operation, it is necessary to first understand classical computing and its use of gates. In classical computing, binary bits "0" and "1" are utilized to store information, and logical circuits are constructed using three primary gates: NOT, AND, and OR. In contrast, quantum computing employs quantum bits, or qubits, to represent information. Qubits are represented using a linear combination of two states, $|0\rangle$ and $|1\rangle$, and can exist in multiple states simultaneously due to the phenomenon of quantum superposition. Therefore, a single qubit can be defined as $|\psi\rangle = \alpha|0\rangle + \beta|1\rangle$, where α and β are complex coefficients, which satisfy $|\alpha|^2 + |\beta|^2 = 1$. In quantum computing, measuring the qubit $|\psi\rangle$ will result in probability of $|\alpha|^2$ and $|\beta|^2$ for states $|0\rangle$ and $|1\rangle$, respectively. Any qubit can be represented in a unit 2-sphere, so called Bloch sphere.

According to Bloch sphere in Fig. 2, a single qubit is represented as $|\psi\rangle = \cos(\frac{\theta}{2})|0\rangle + e^{i\phi} \sin(\frac{\theta}{2})|1\rangle$. Therefore, the amplitude coefficients α and β are $\cos(\theta/2)$, and $e^{i\phi} \sin(\theta/2)$, respectively.

A $2^n \times 2^n$ unitary matrix is used to describe a gate acting on n qubits. Furthermore, in a quantum system composed of two qubits, there exist four basis states: $|00\rangle$, $|01\rangle$, $|10\rangle$, and $|11\rangle$.

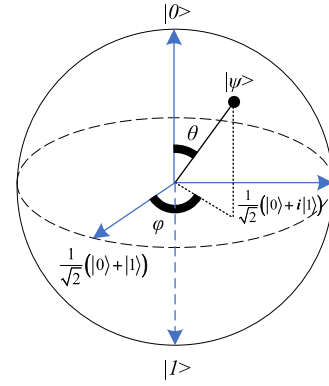


Fig. 2. A single qubit representation in Bloch sphere.

For a system composed of n qubits, there are 2^n basis states, each with complex coefficients. Quantum gates are fundamental blocks of quantum circuits operating on input qubits. The qubits are usually initialized to $|0\rangle$, and quantum gates act on the input qubits. At the end of quantum circuit, there exists a measurement unit to measure the output quantum states.

B. Quantum Optimization Procedure

In this subsection, the optimization model that is utilized by QA is discussed. Additionally, the process of preparing a classical optimization problem to be solved by quantum annealing-inspired method is explained.

Quantum annealing is a type of optimization algorithm that is implemented on D-Wave quantum computers. It is particularly useful for solving combinatorial optimization problems, by searching for near-optimal or global optima [22], [26], [27]. The quantum processors units (QPUs) of D-Wave computers are designed to perform quantum annealing and are adaptable to solve QUBO problems. A classical QUBO problem can be defined as follows:

$$x = \underset{x}{\operatorname{argmin}} (x^T Q x + C x), \quad (10)$$

where, x is a $N \times 1$ vector of binary decision variables. Real-valued matrices Q and C are $N \times N$ and $1 \times N$ vectors, respectively.

The minimum value of the corresponding objective function in an optimization problem is equivalent to finding the ground state of an Ising Hamiltonian [28], [29]. To achieve the Ising model of a QUBO problem, a graph $G = (V, E)$ is given in Fig. 3.

The Ising Hamiltonian model is constructed using the vertices and edges of a graph G , which represents an electric grid with nodes and lines. The nodes and lines of the grid are respectively represented by the vertices and edges of the graph. The binary decision variables are represented by the qubits associated with the vertices. Each vertex is associated with an external magnetic field, denoted by q , and a spin value $\xi = \pm 1$. The interaction between two qubits k and j is described by the coupling between their associated vertices through the edge between them (L_{kj}). Based on this graph, the Ising Hamiltonian model \mathcal{H} can be

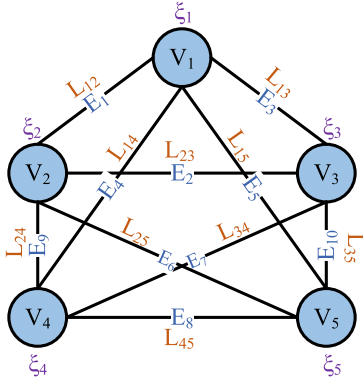


Fig. 3. Representation of an Ising model in a sample graph.

formulated as follows:

$$\mathcal{H} = \sum_{k=1}^N \sum_{j=1, j \neq k}^N L_{kj} \cdot \xi_k \cdot \xi_j + \sum_{k \in V} q_k \cdot \xi_k. \quad (11)$$

where, the first term of Ising model in (11) indicates the interaction/coupling between two qubits while the second term has to do with the local field caused by external magnetic with a spin. To map the classical QUBO problem to the Hamiltonian Ising model, the binary decision variables $x \in \{0, +1\}$ in (10) should be replaced by spin variables $\xi \in \{-1, +1\}$ in (11). To fulfill this conversion, the transformation $x = \frac{\xi+1}{2}$ is employed. This conversion results in:

$$L_{kj} = \frac{1}{4} Q_{kj}, \quad \forall (k, j) \in E, \quad (12a)$$

$$q_k = \frac{1}{2} \left(C_k + \sum_j Q_{kj} \right), \quad \forall k \in V. \quad (12b)$$

According to the adiabatic theorem of quantum mechanics, a system can be expressed by a time-varying Hamiltonian, $H = A(t)\mathcal{H}_0 + B(t)\mathcal{H}_p$, in which the path functions of QA are represented by A and B [30], [31]. In the first step of QA, the system is initialized such that $A(0) = 1$, and $B(0) = 0$. While $A(t)$ changes from $A(0) = 1$ to $A(T) = 0$ as the final value at time T , the value of $B(t)$ increases from $B(0) = 0$ to $B(T) = 1$. Consequently, the Hamiltonian of Ising model is changed from $H(0) = \mathcal{H}_0$ to $H(T) = \mathcal{H}_p$. A system Hamiltonian with the known ground state is initialized and prepared as follows:

$$\mathcal{H}_0 = \sum_{k=1}^N \sigma_k^x, \quad (13)$$

where, Pauli-x operator $\sigma_k^x = \begin{bmatrix} 0 & 1 \\ 1 & 0 \end{bmatrix}$ is applied to qubit k .

As mentioned, the system evolves over time under a slowly changing Hamiltonian toward problem Hamiltonian \mathcal{H}_p that encodes the problem to be solved:

$$\mathcal{H}_p = \sum_{k=1}^N \sum_{j=1, j \neq k}^N L_{kj} \cdot \sigma_k^z \cdot \sigma_j^z + \sum_{k \in V} q_k \cdot \sigma_k^z, \quad (14)$$

where, Pauli-z operator $\sigma_k^z = \begin{bmatrix} 1 & 0 \\ 0 & -1 \end{bmatrix}$ is applied to qubit k .

The problem Hamiltonian \mathcal{H}_p is the classical Ising model in (11), and therefore, the problem Hamiltonian's eigenvectors are used to obtain the solution of the Ising model.

According to the adiabatic theorem of quantum mechanics, if the required transition (annealing) time from \mathcal{H}_0 to \mathcal{H}_p is sufficiently slow, the system guarantees the ground state, meaning that the optimal solution is achieved [32], [33].

C. Quantum Model for Resilient Microgrids Formation

In this subsection, the quantum-inspired resilient MGs formation model is developed and the optimization solution using QA in a D-Wave machine is discussed. In the context of quantum annealing and the Constrained Quadratic Model (CQM) solver, specific steps are undertaken to adapt classical optimization problems for quantum optimization methods. In [18], [19], these steps are applied to unit commitment problem prior to utilizing the quantum distributed method for solving. The fundamental procedures for converting a classical problem for the CQM solver can be outlined as follows:

- Convert inequality constraints to equality constraints by introducing slack variables.
- Introduce penalty functions for each inequality constraint in the objective function, with penalty terms as functions of slack variables and penalty parameters.
- Form the combined objective function by adding the original objective function and penalty terms.
- Convert the modified objective function and equality constraints into a quadratic form, aligning with the QUBO problems typically processed by quantum annealers.

Following the application of the mentioned transformations, the objective function can be translated into the Ising model.

Objective Function: The objective function (9) should be mapped to the Ising model by converting the binary variables into spins using the transformation $x = \frac{\xi+1}{2}$:

$$\max_{\xi} \mathcal{H}_{obj} : \max_{\xi} \sum_{i \in B^*} \sum_{m \in M} c_i \cdot \frac{1 + \xi_{im}^e}{2} \cdot P_{i,m}^L, \quad (15)$$

where, ξ_{im}^e is the spin associated with energized load i in MG m .

Node Belonging Constraint: The constraint Hamiltonian associated with classical constraint (1) is written as follows:

$$\mathcal{H}_{c1} = \lambda_1 \sum_{i \in B^*} \left(\sum_{m \in M} \frac{1 + \xi_{im}^w}{2} - 1 \right)^2, \quad (16)$$

where, ξ_{im}^w is the spin for node i in MG m . Furthermore, since the problem should be in unconstrained form, the existing constraints should be added to the objective function in a quadratic form by a penalty coefficient. Hence, λ_1 is the penalty coefficient of node belonging constraint.

Line Belonging Constraint: The line belonging constraint (3a)–(3c) is transformed to the Hamiltonian model as follows:

$$\mathcal{H}_{c2} = \lambda_2 \sum_{i, \tilde{i} \in B^*} \sum_{m \in M} \left(\frac{1 + \xi_{i\tilde{i}m}^l}{2} - \frac{1 + \xi_{im}^w}{2} + y_{1, i\tilde{i}m} \right)^2, \quad (17a)$$

$$\mathcal{H}_{c3} = \lambda_3 \sum_{i, \tilde{i} \in B^*} \sum_{m \in M} \left(\frac{1 + \xi_{i\tilde{i}m}^l}{2} - \frac{1 + \xi_{im}^w}{2} + y_{2, i\tilde{i}m} \right)^2, \quad (17b)$$

$$\mathcal{H}_{c4} = \lambda_4 \sum_{i, \tilde{i} \in B^*} \sum_{m \in M} \left(\frac{1 + \xi_{im}^w}{2} + \frac{1 + \xi_{im}^w}{2} - \frac{1 + \xi_{i\tilde{i}m}^l}{2} - 1 + y_{3, i\tilde{i}m} \right)^2, \quad (17c)$$

where, $\xi_{i\tilde{i}m}^l$ is the spin associated with distribution line l between nodes i and \tilde{i} in MG m . ξ_{im}^w is the spin for node i in MG m . Moreover, the penalty terms are indicated by λ_2 , λ_3 and λ_4 . The non-negative slack variables corresponding to inequality constraints (3a)–(3c) are represented by $y_{1, i\tilde{i}m}$, $y_{2, i\tilde{i}m}$ and $y_{3, i\tilde{i}m}$, respectively.

Node Connectivity Constraint: To ensure the connectivity of nodes in a microgrid and capture the radial topology of a distribution system, classical constraint (4) should be converted to the following constraint Hamiltonian:

$$\mathcal{H}_{c5} = \lambda_5 \sum_{i \in B^*} \sum_{\tilde{i} \in B^*} \sum_{m \in M} \left(\frac{1 + \xi_{im}^w}{2} - \frac{1 + \xi_{im}^w}{2} + y_{4, i\tilde{i}m} \right)^2, \quad (18)$$

where, λ_5 is the penalty term associated with node connectivity constraint. Furthermore, to ensure proper handling of the inequality constraint (4), the non-negative slack variables $y_{4, i\tilde{i}m}$ are introduced.

Energized Loads Constraint: The Hamiltonian of energized loads constraint in (6a–6c) is represented as follows:

$$\mathcal{H}_{c6} = \lambda_6 \sum_{i \in B^*} \sum_{m \in M} \left(\frac{1 + \xi_{im}^e}{2} - \frac{1 + \xi_{im}^w}{2} + y_{5, im} \right)^2, \quad (19a)$$

$$\mathcal{H}_{c7} = \lambda_7 \sum_{i \in B^*} \sum_{m \in M} \left(\frac{1 + \xi_{im}^e}{2} - \frac{1 + \xi_{im}^s}{2} + y_{6, im} \right)^2, \quad (19b)$$

$$\mathcal{H}_{c8} = \lambda_8 \sum_{i \in B^*} \sum_{m \in M} \left(\frac{1 + \xi_{im}^w}{2} + \frac{1 + \xi_{im}^s}{2} - \frac{1 + \xi_{im}^e}{2} - 1 + y_{7, im} \right)^2, \quad (19c)$$

where, λ_6 , λ_7 and λ_8 are penalty coefficients of energized loads constraint. Moreover, $y_{5, im}$, $y_{6, im}$ and $y_{7, im}$ are non-negative slack variables of constraints (6a)–(6c), respectively.

DistFlow Constraint: In quantum annealing for solving the load restoration problem through MGs formation, a common practice is to convert the problem, which encompasses both continuous and binary decision variables, into a QUBO problem. In accordance with (7a), (7b), and (7c), where P^{flow} , Q^{flow} and V are continuous variables, the integration of continuous variables into the Ising model involves a discretization process. The following steps outline how to incorporate continuous variables into the Ising model for the load restoration problem:

- *Choose discretization intervals:* Determine the granularity of discretization by defining intervals for converting continuous variables into discrete values.
- *Discretization formula:* Develop a formula for discretization to map each continuous variable to its discrete representation.
- *Integer representation:* Represent the discrete values as integers, ensuring the preservation of the original continuous variable's order. A binary encoding scheme is employed to represent continuous variables as a combination of binary variables. Let ϖ denote a continuous variable requiring discretization. ϖ is represented using N binary variables b_k , each capable of taking values of 0 or 1. The binary encoding is achieved through the equation $\varpi = \sum_{k=1}^N b_k \cdot 2^{k-1}$, where the value of ϖ is determined by summing the products of each binary variable with its corresponding power of 2. The precision and range of values that ϖ can assume are controlled by adjusting the number of binary variables N . In the Ising model framework, the binary variables b_k can be interpreted as spin variables ξ that take values in $-1, +1$, where each spin variable ξ_k is defined as $\xi_k = 2\varpi_k - 1$.
- *Adjust Objective Function:* Modify the objective function to operate on discretized values, adapting coefficients, scaling factors, or introducing penalties as needed for compatibility with discrete decision variables.
- *Quantum Annealing Formulation:* Formulate the load restoration problem with discretized decision variables and an adjusted objective function in the Ising model, suitable for quantum annealing.
- *Post-processing:* After quantum annealing, map binary solutions back to continuous values using the inverse of the discretization formula.

In the linearized DistFlow model of the load restoration problem, the variables $\hat{P}_{i,m}^{flow}$, $\hat{Q}_{i,m}^{flow}$ and $\hat{V}_{i,m}$ represent the discretized forms of continuous variables $P_{i,m}^{flow}$, $Q_{i,m}^{flow}$ and $V_{i,m}$ respectively. The spins $\hat{\xi}_{im}^{Pflow}$ and $\hat{\xi}_{i-\tilde{i},m}^{Pflow}$ correspond to the spins related to $\hat{P}_{i,m}^{flow}$ and $\hat{P}_{i-\tilde{i},m}^{flow}$. Similarly, the spins for $\hat{Q}_{i,m}^{flow}$ and $\hat{Q}_{i-\tilde{i},m}^{flow}$ are denoted by $\hat{\xi}_{im}^{Qflow}$ and $\hat{\xi}_{i-\tilde{i},m}^{Qflow}$, respectively. The spin $\hat{\xi}_{im}^V$ is the spin associated with $\hat{V}_{i,m}$.

The Hamiltonian of DistFlow model is written as follows:

$$\mathcal{H}_{c9} = \lambda_9 \sum_{i \in B^*} \sum_{m \in M} \left(\frac{1 + \hat{\xi}_{im}^{Pflow}}{2} - \sum_{\tilde{i}} \frac{1 + \hat{\xi}_{i-\tilde{i},m}^{Pflow}}{2} - \frac{1 + \xi_{im}^e}{2} \cdot P_{i,m}^L \right)^2, \quad (20a)$$

$$\mathcal{H}_{c10} = \lambda_{10} \sum_{i \in B^*} \sum_{m \in M} \left(\frac{1 + \hat{\xi}_{im}^{Qflow}}{2} - \sum_{\hat{i}} \frac{1 + \hat{\xi}_{i-\hat{i},m}}{2} - \frac{1 + \xi_{im}^e}{2} \cdot Q_{i,m}^L \right)^2, \quad (20b)$$

$$\mathcal{H}_{c11} = \lambda_{11} \sum_{i \in B^*} \sum_{\tilde{i} \in B^*} \sum_{m \in M} \left(\frac{1 + \hat{\xi}_{im}^V}{2} - \frac{1 + \hat{\xi}_{\tilde{i}m}^V}{2} + \frac{R_{i-\tilde{i}} \cdot \frac{1 + \hat{\xi}_{im}^{Pflow}}{2} + X_{i-\tilde{i}} \cdot \frac{1 + \hat{\xi}_{im}^{Qflow}}{2}}{V_{0,m}} \right)^2, \quad (20c)$$

where, λ_9 , λ_{10} and λ_{11} are penalty terms used for DistFlow constraint.

Line Flow Constraint: In-flow real and reactive powers have the following Hamiltonian model:

$$\mathcal{H}_{c12} = \lambda_{12} \sum_{i \in B^*} \sum_{m \in M} \left(\frac{1 + \hat{\xi}_{im}^{Pflow}}{2} - \frac{1 + \xi_{im}^w}{2} \cdot \bar{P}_{DG,m} + y_{8,im} \right)^2, \quad (21a)$$

$$\mathcal{H}_{c13} = \lambda_{13} \sum_{i \in B^*} \sum_{m \in M} \left(\frac{1 + \hat{\xi}_{im}^{Qflow}}{2} - \frac{1 + \xi_{im}^w}{2} \cdot \bar{Q}_{DG,m} + y_{9,im} \right)^2, \quad (21b)$$

$$\mathcal{H}_{c14} = \lambda_{14} \sum_{i \in B^*} \sum_{m \in M} \left(\frac{1 + \hat{\xi}_{im}^V}{2} - \sum_{k \in V} \frac{1 + \xi_{im}^w}{2} \cdot V_{0,m} + y_{10,im} \right)^2, \quad (21c)$$

where, the penalty coefficients of line flow constraint are represented by λ_{12} , λ_{13} and λ_{14} . The non-negative slack variables of line flow constraints are indicated by $y_{8,im}$, $y_{9,im}$ and $y_{10,im}$.

It should be mentioned that estimating penalty coefficients (λ) for D-Wave's CQM involves an iterative process. Starting with an initial value, the solver undergoes runs with different scaling factors, aiming to balance constraints and minimize energy. Solution quality is assessed iteratively, considering problem-specific characteristics. Optimal coefficients are problem-specific and refined based on insights from previous runs. Leveraging D-Wave Leap's hybrid solvers provides valuable perspectives in this estimation process.

Once the QUBO objective function and constraints are mapped to a Hamiltonian model, the next step is to construct the problem Hamiltonian, also known as the total energy function, which can be used to find the minimum energy of the system using QA:

$$\mathcal{H}_p = -\mathcal{H}_{obj} + \sum_{d=1}^D \mathcal{H}_{cd}, \quad (22)$$

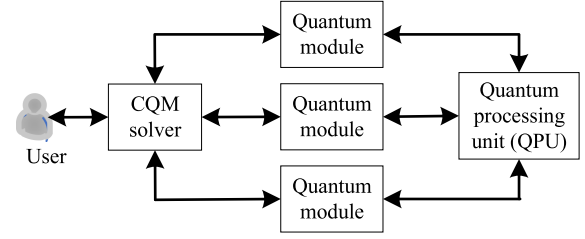


Fig. 4. The structure of CQM solver.

where, D is the total number of constraints Hamiltonian. Since the classical optimization problem in (9) is a maximization problem, the sign of \mathcal{H}_{obj} is changed to negative to be considered as a minimization problem solvable by QA.

D. The Structure of D-Wave Hybrid Solvers

The ‘Advantage’ quantum processor of D-Wave contains at least 5000 qubits, while the previous 2000Q processor has up to 2048 qubits. Furthermore, compared to the D-Wave 2000Q system, the new released ‘Advantage’ processor has 15 number of couplers per qubit, which is 2.5 times more than its predecessor [34]. Large number of qubits along with high connectivity and coupling between qubits are the key factors in solving large scale optimization problems using QA. Current D-Wave hybrid solvers are capable of solving a complex problem in presence of one million decision variables and 100,000 constraints.

The load restoration problem is solved by using a hybrid solver called CQM solver from D-Wave, as shown in the structure depicted in Fig. 4.

The CQM solver utilizes several classical solvers that are executed on classical CPUs and GPUs and perform a search for high-quality solutions. A quantum module is present in each classical solver and it is responsible for crafting quantum inquiries and transmitting them to the D-Wave quantum processing unit QPU. The responses received from the D-Wave QPU in response to the quantum queries can be utilized to direct the heuristic search or enhance the quality of the existing set of solutions.

IV. NUMERICAL RESULTS

This section explores the efficacy of quantum annealing-inspired method in solving the MILP problem by D-Wave’s hybrid quantum-classical solver. Furthermore, the classical solver Gurobi is run on a laptop equipped with an Intel Core(TM) i9-10885H CPU running at a base frequency of 2.40 GHz. Two case studies, modified IEEE 37-bus system [35] and modified IEEE 240-bus system [36], are utilized.

A. IEEE 37-Bus System

The single-line diagram of modified IEEE 37-bus distribution system is depicted in Fig. 5.

This case study involves three distributed generators located at nodes 2, 14, and 19, each with a maximum real power generation capacity of 252.53 kW, 120.42 kW, and 202.99 kW, and a maximum generated reactive power of 46.31 kVar, 171.72 kVar,

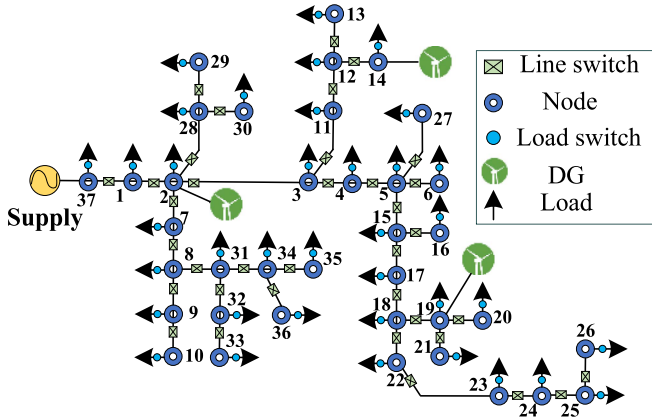


Fig. 5. The single-line diagram of modified IEEE 37-bus distribution system.

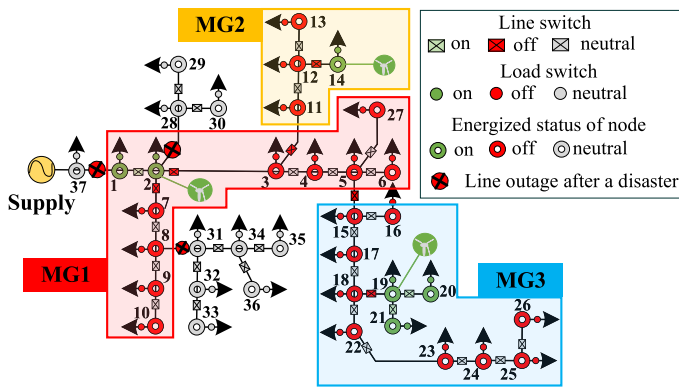


Fig. 6. Microgrids formation after a natural disaster.

TABLE I
BELONGING OF SYSTEM NODES TO MGs AND ENERGIZED STATUS AND VOLTAGE LEVEL OF NODES AFTER RESILIENT MGs FORMATION

MG	Node	Energized node (Voltage)
MG1	1,2,3,4,5,6,7,8,9,10,27	1,2 (220v),(220v)
MG2	11,12,13,14	14 (220v)
MG3	15,16,17,18,19,20,21,22,23,24,25,26	19,20,21 (220v),(219.9v),(220v)

and 197.48 kVar, respectively. The line and load switches can be either on (1) or off (0), and the objective function assigns a priority weight (c) to each load, indicating its importance in being restored after a natural disaster. The load weights and amounts of real and reactive loads from [5] are used in this case study.

Fig. 6 shows the new topology of the distribution system after the formation of MGs due to a natural disaster. In Fig. 6, it can be observed that three lines are unavailable due to the natural disaster, and their corresponding line switches have been turned off. These lines are located between nodes 1-37, 2-28, and 8-31. The remaining part of the distribution grid is used to form three microgrids for restoring the loads. Each microgrid is equipped with a distributed generation unit to supply power to its loads. The nodes are assigned to the MGs as described in Table I.

The results of the resilient MGs formation, as shown in Fig. 6 and Table I, determines the switching mode of loads and lines to allocate nodes and lines for each MG. Furthermore, the identification of energized loads for each MG after the disaster, along with the voltage level of energized loads at buses, is carried out.

The minimum energy level of the system, which is equivalent to the minimum value of the objective function, is found to be -700.4632 using D-Wave's hybrid quantum-classical solver. This value is consistent with the minimum value obtained by the classical solver Gurobi.

The active and reactive powers sent by different nodes in their respective microgrids after resilient MGs formation are as follows: in MG1, nodes 1 and 2 send 30.4 kW and 49.01 kW of real power, and 5.09 kVar and 28.69 kVar of reactive power, respectively. In MG2, the real and reactive powers sent by node 14 are 41.18 kW and 7.45 kVar, respectively. Similarly, in MG3, nodes 19, 20, and 21 send 60.14 kW, 35.12 kW, and 12.45 kW of real power, respectively, along with 41.49 kVar, 19.28 kVar, and 13.76 kVar of reactive power, respectively.

B. IEEE 240-Bus Distribution System

To validate the performance of Wave's hybrid quantum-classical solver on large-scale systems, an IEEE 240-bus distribution system with a single-line diagram depicted in Fig. 7 is used. The test system consists of 240 buses and three feeders. 17-node feeder, 60-node feeder, and 162-node feeder entail 2, 8, and 15 DGs, respectively.

In this case study, three scenarios are considered. In the first scenario, which only includes the first 17-node test feeder, the MGs formation problem is solved. In the second scenario, test feeders with 17 nodes and 60 nodes are utilized. In the third scenario, the MGs formation problem is solved in presence of all feeders. In each scenario, the optimization solution obtained by quantum annealing-inspired method is compared with those from classical solver.

First scenario: 17-node test feeder: In this scenario, two DGs are located in buses 2 and 8 with the maximum real and reactive powers to be 100 kW and 50 kVar, respectively. The new reconfiguration of the system after a disaster is achieved, as shown in Fig. 8.

After the MGs formation, the first feeder is split into two MGs with a DG in each one to restore critical loads. While DG1 and DG2 produce 92.91 kW and 57.90 kW of real power, respectively, the generated reactive powers by the DGs are 43.50 kVar and 29.69 kVar, respectively.

Quantum annealing-inspired method using D-Wave's hybrid quantum-classical solver and classical solver using Gurobi achieve the same solution, and the value of objective function, which is the sum of picked-up weighted critical loads, becomes -752.5489. The low-energy states of the critical load restoration problem are sampled by the hybrid CQM sampler. The hybrid CQM sampler sampled from 103 solutions among which 73 feasible solutions are achieved. Because of the probabilistic nature of solutions obtained by D-Wave's hybrid solver, the

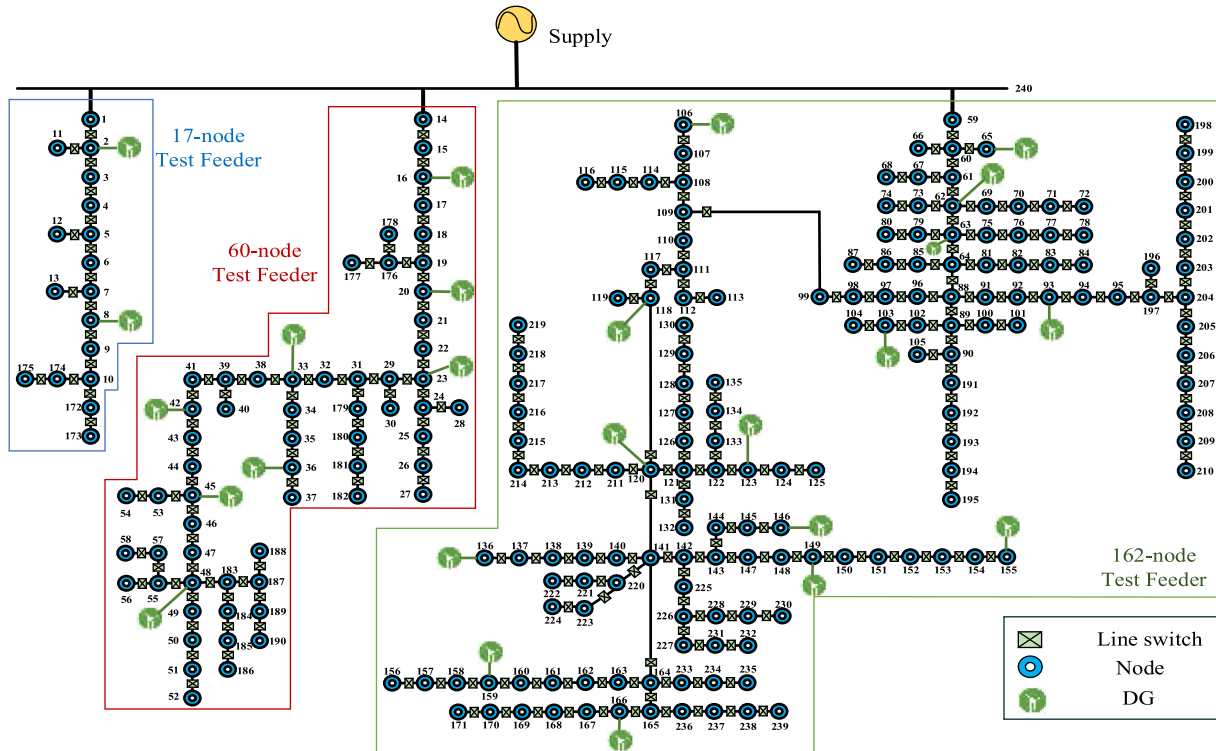


Fig. 7. The single-line diagram of modified IEEE 240-bus distribution system.

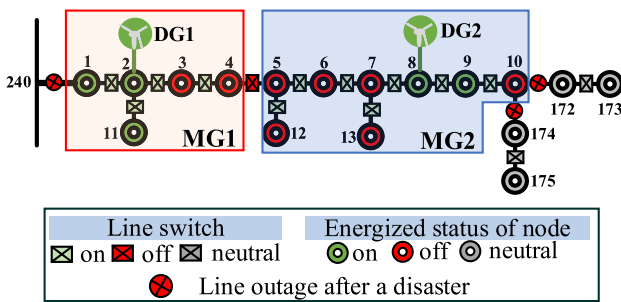


Fig. 8. Microgrids formation after a natural disaster in the 17-node test feeder (first scenario).

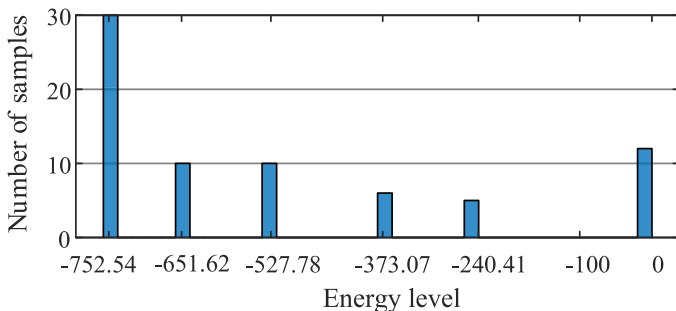


Fig. 9. Energy level of MGs formation problem for different samples in the 17-node test feeder (first scenario).

number of samples for each achieved energy level or solution is depicted in Fig. 9.

According to the samples in Fig. 9, the best solution obtained by D-Wave’s hybrid quantum-classical solver is -752.5489 ,

which is exactly the same value of objective function from classical solver Gurobi. Due to the probabilistic nature of the quantum computing, the probability of this energy level is 41.10%.

After the formation of MGs, the loads in buses 1, 2, and 11 of MG1 and the loads in buses 8 and 9 of MG2 are successfully restored.

Second scenario: 17-node test feeder + 60-node test feeder: In this scenario, 17-node test feeder and 60-node test feeder are involved. The second feeder comprises 60 buses and 8 DGs. The new configuration of the distribution system including two test feeders based on annealing-based quantum computing results is shown in Fig. 10.

According to the resilient distribution system structure after a disaster based on quantum annealing-inspired method, 201.26 kW real power and 77.10 kVar reactive power are restored inside MG3. MG4 formation results in real and reactive critical load restoration of MG4 with the values of 167.71 kW and 95.56 kVar, respectively. The results obtained by D-Wave’s hybrid quantum-classical solver are the same with those from the classical solver Gurobi after forming MG1, MG2, MG3 and MG4. However, when the system is become larger, the results from quantum annealing-inspired method are promising and efficient than the classical solver. The output of D-Wave’s hybrid quantum-classical solver for MG5 shows that 173.97 kW of real and 78.46 kVar of reactive critical loads are restored after forming MG5. In comparison, the classical solver returns 145.32 kW of real and 58.44 kVar of reactive critical loads restored in MG5.

In Fig. 11, the energy level of the problem is depicted, where the CQM solver returns 65 feasible samples.

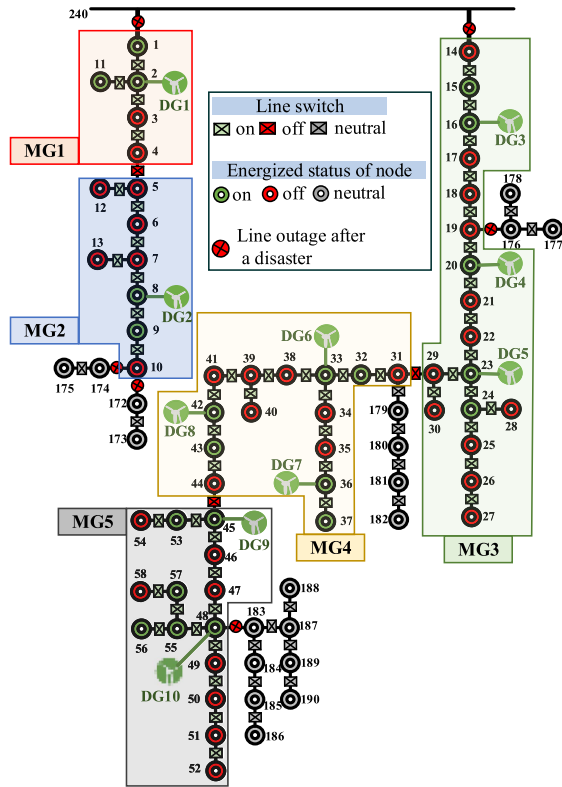


Fig. 10. Microgrids formation after a natural disaster entailing two feeders (second scenario).

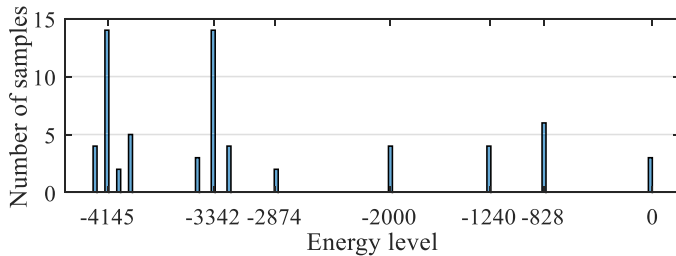


Fig. 11. Energy level of MGs formation entailing two feeders considering different samples (second scenario).

The energy level of -4145.45 is achieved with the probability of 21.5% using quantum annealing-inspired method, while the minimum value of objective function is -4031.14 using classical solver Gurobi.

Third scenario: The distribution system with three test feeders: In this scenario, all feeders and nodes of the 240-bus distribution system, including 25 DGs, are taken into account. Fig. 12 displays the new configuration of the distribution system resulting from the formation of resilient microgrids in response to a catastrophe.

Table II presents details regarding the total restored critical loads by DGs, the corresponding locations of restored loads for each microgrid, and the voltage levels of energized loads at buses. Table II demonstrates that the real and reactive powers generated by the DGs determine the amount of real and reactive critical loads restored. In feeder 1, two microgrids are formed,

TABLE II
RESULTS OF LOAD RESTORATION AFTER MGs FORMATION

MG	DG	Real load restored by DG (kW)	Reactive load restored by DG (kVar)	Restored loads location (Voltage)
MG1	DG1	92.91	43.50	1,2,11 (219.8,220,219.8) _v
MG2	DG2	57.90	29.69	8,9 (220,210) _v
MG3	DG3	71.07	28.37	15,16 (210,220) _v
	DG4	35.12	19.28	20 (220) _v
	DG5	95.07	29.45	23,24 (220,210) _v
MG4	DG6	63.40	29.45	32,33 (210,220) _v
	DG7	20.63	40.65	36,37 (220,219.9) _v
MG5	DG8	83.68	37.46	42,43 (220,210) _v
	DG9	74.89	31.12	45,53 (220,210) _v
MG6	DG10	99.08	47.34	48,55,56,57 (220,210,1,210,210)
	DG11	70.81	32.99	62,69,70 (220,210,2,210) _v
MG7	DG12	12.58	19.25	65 (220) _v
	DG13	99.32	48.11	63,64,79 (220,210,210) _v
MG8	DG14	60.14	41.49	93,94,95 (220,210,1,210) _v
	DG15	12.73	24.77	103 (220) _v
MG9	DG16	29.58	9.90	106 (220) _v
	DG17	64	44.88	118,119 (220,219.9) _v
MG10	DG18	31.51	11.29	120 (220) _v
	DG19	95.93	18.67	123,124,125 (220,210,2,210) _v
MG11	DG20	7.41	15.54	136 (220) _v
	DG21	29.37	4.35	146 (220) _v
MG12	DG22	51.03	45.74	147,148,149 (210,210,2,220) _v
	DG23	37.61	26.48	155 (220) _v
MG13	DG24	62.79	44.01	158,159 (210,220) _v
	DG25	67.63	46.29	166,167,168,169 (220,210,2,210,210)

each consisting of one DG. These microgrids restore a total of 92.91 kW and 57.90 kW of real critical loads and 43.50 kVar and 29.69 kVar of reactive critical loads, respectively. In feeder 2, the formation of three microgrids (MG3, MG4, and MG5) restores a total of 201.26 kW and 77.10 kVar, 167.71 kW and 107.56 kVar, and 173.97 kW and 78.46 kVar of critical loads, respectively. The formation of microgrids MG6 to MG13 in feeder three results in the restoration of the following total loads: 83.39 kW and 52.24 kVar for MG6, 99.32 kW and 48.11 kVar for MG7, 72.87 kW and 66.26 kVar for MG8, 93.58 kW and 54.78 kVar for MG9, 127.44 kW and 29.96 kVar for MG10, 36.78 kW and 19.89 kVar for MG11, 88.64 kW and 72.22 kVar for MG12, and 130.42 kW and 90.30 kVar for MG13. Additionally, Table II includes the voltage levels of energized loads, all of which fall within predetermined limits.

Fig. 13 displays the samples returned by the CQM solver for each energy level of the system.

The quantum annealing-inspired method returns a weighted load restoration of 8030.77 kW with a probability of 27.7%, while the classical solver Gurobi provides a solution of 7229.98 kW. This comparison highlights the potential advantage of using quantum annealing-inspired method in solving complex combinatorial problems compared to classical methods. The goal of D-Wave hybrid solver is to take advantage of the strengths of classical and quantum optimization algorithms, as well as

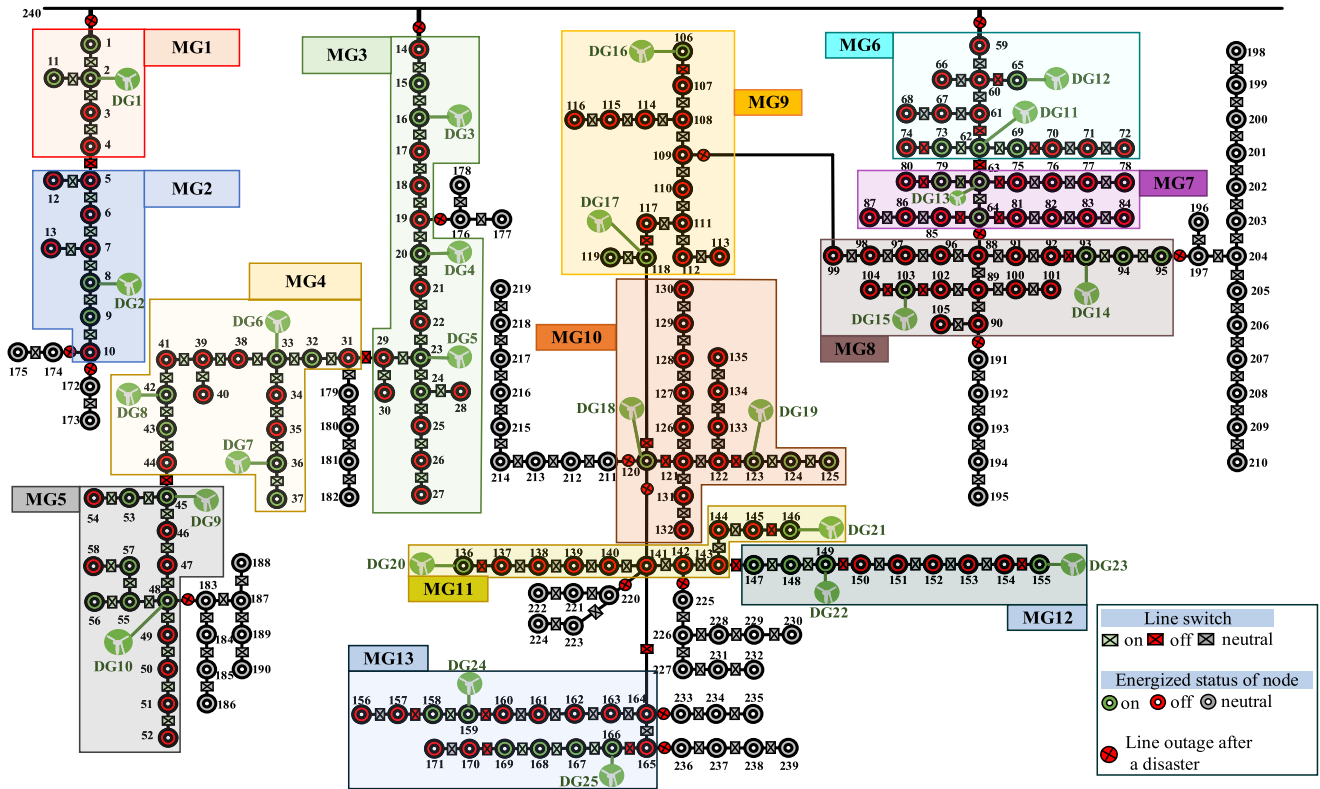


Fig. 12. The formation of microgrids after a natural disaster in presence of all feeders (third scenario).

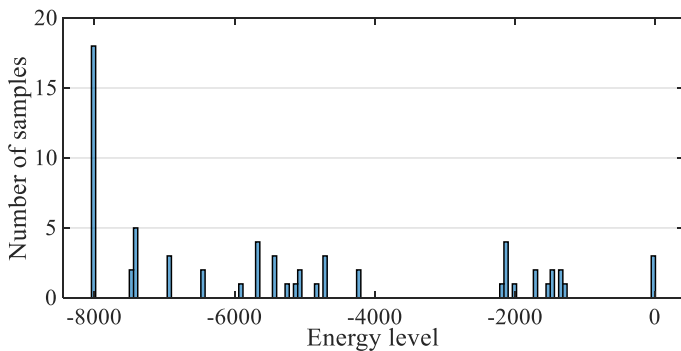


Fig. 13. Energy level of MGs formation problem in the 240-bus distribution system (third scenario).

TABLE III
RUNNING TIME OF QUANTUM ANNEALING-INSPIRED METHOD AND CLASSICAL SOLVER IN DIFFERENT SCENARIOS

Method	First scenario	Second scenario	Third scenario
Quantum Annealing	0.016s	0.032s	0.217s
Gurobi	0.278s	1.17s	8.32s

parallelism of quantum computing to improve solutions to complex problems. By combining classical optimization methods with quantum annealing, these solvers aim to achieve a balance between solution quality and computational efficiency, making them a valuable tool for resolving combinatorial optimization challenges. In Table III, a comparison of the running time between the D-Wave’s hybrid quantum-classical solver and

classical solver is presented for three scenarios in the 240-bus distribution system.

As indicated by Table III, the time it takes for the QPU to solve the optimization problem is faster than the classical solver (Gurobi), even as the size of the problem increases. This highlights the advantage of using D-Wave hybrid solvers for complex problems, as they offer faster solution times compared to classical solvers.

Quantum computing’s faster calculations in MGs formation, enhancing distribution network resilience, result from key factors. Quantum parallelism enables simultaneous exploration of multiple configurations, expediting optimization for complex problems. Quantum tunneling efficiently navigates complex landscapes, ensuring quicker convergence to optimal solutions. Its ability to handle non-continuous variables is crucial for determining microgrid configurations and network allocation. Additionally, hybrid approaches, combining classical and quantum processing, leverage quantum tunneling for efficient exploration and optimization in complex problems like load restoration through MGs formation.

V. CONCLUSION

To address large-scale combinatorial optimization problems, leveraging quantum annealing-inspired computing platforms shows promise in tackling a variety of power system challenges. Combinatorially complex Operational optimization problems including non-continuous decision variables are good candidates for quantum annealing-inspired methods to

overcome the barriers of current classical methods. In this paper, to take advantage of quantum optimization methods, the quantum-enabled resilient MGs formation and load restoration problem was developed by deriving the Ising Hamiltonian model. Then, to find the minimum value of the objective function, the ground state of the Hamiltonian model was obtained, which is the minimum energy level of the system. To restore the critical loads in the distribution system, MGs formation was considered as an effective strategy where the switching status (0/1) of distribution lines and loads were deciding factors in keeping the critical loads energized after natural disasters. For the first time, practical system restorations considering DGs, various switches as well as MGs formation, power flow and operational constraints are realized on real quantum annealing-based quantum computers. Results obtained by quantum annealing-inspired method demonstrate the accuracy of this computing platform compared to the classical solver.

ACKNOWLEDGMENT

The United States Government has a royalty-free license throughout the world in all copyrightable material contained herein.

REFERENCES

- [1] A. B. Smith, "US billion-dollar weather and climate disasters, 1980-present," NOAA National Centers for Environmental Information, 2022. [Online]. Available: <https://www.ncei.noaa.gov/access/billions/events.pdf>
- [2] X. Liu, M. Shahidehpour, Z. Li, X. Liu, Y. Cao, and Z. Bie, "Microgrids for enhancing the power grid resilience in extreme conditions," *IEEE Trans. Smart Grid*, vol. 8, no. 2, pp. 589–597, Mar. 2017.
- [3] P. Zhang, *Networked Microgrids*. Cambridge, U.K.: Cambridge Univ. Press, 2021.
- [4] P. Zhang, *Microgrids: Theory and Practice*. Hoboken, NJ, USA: Wiley, 2024.
- [5] C. Chen, J. Wang, F. Qiu, and D. Zhao, "Resilient distribution system by microgrids formation after natural disasters," *IEEE Trans. Smart Grid*, vol. 7, no. 2, pp. 958–966, Mar. 2016.
- [6] Y. Xu, C.-C. Liu, K. P. Schneider, F. K. Tuffner, and D. T. Ton, "Microgrids for service restoration to critical load in a resilient distribution system," *IEEE Trans. Smart Grid*, vol. 9, no. 1, pp. 426–437, Jan. 2018.
- [7] H. Gao, Y. Chen, Y. Xu, and C.-C. Liu, "Resilience-oriented critical load restoration using microgrids in distribution systems," *IEEE Trans. Smart Grid*, vol. 7, no. 6, pp. 2837–2848, Nov. 2016.
- [8] S. Poudel and A. Dubey, "Critical load restoration using distributed energy resources for resilient power distribution system," *IEEE Trans. Power Syst.*, vol. 34, no. 1, pp. 52–63, Jan. 2019.
- [9] A. S. Kahnemouei and S. Lottifard, "Enhancing resilience of distribution networks by coordinating microgrids and demand response programs in service restoration," *IEEE Syst. J.*, vol. 16, no. 2, pp. 3048–3059, Jun. 2022.
- [10] J. Li, X.-Y. Ma, C.-C. Liu, and K. P. Schneider, "Distribution system restoration with microgrids using spanning tree search," *IEEE Trans. Power Syst.*, vol. 29, no. 6, pp. 3021–3029, Nov. 2014.
- [11] S. Cai, Y. Xie, Q. Wu, M. Zhang, X. Jin, and Z. Xiang, "Distributionally robust microgrid formation approach for service restoration under random contingency," *IEEE Trans. Smart Grid*, vol. 12, no. 6, pp. 4926–4937, Nov. 2021.
- [12] M. Song, R. R. Nejad, and W. Sun, "Robust distribution system load restoration with time-dependent cold load pickup," *IEEE Trans. Power Syst.*, vol. 36, no. 4, pp. 3204–3215, Jul. 2021.
- [13] Y. Xu and W. Liu, "Novel multiagent based load restoration algorithm for microgrids," *IEEE Trans. Smart Grid*, vol. 2, no. 1, pp. 152–161, Mar. 2011.
- [14] Y. Wang et al., "Coordinating multiple sources for service restoration to enhance resilience of distribution systems," *IEEE Trans. Smart Grid*, vol. 10, no. 5, pp. 5781–5793, Sep. 2019.
- [15] Y. Li, J. Xiao, C. Chen, Y. Tan, and Y. Cao, "Service restoration model with mixed-integer second-order cone programming for distribution network with distributed generations," *IEEE Trans. Smart Grid*, vol. 10, no. 4, pp. 4138–4150, Jul. 2019.
- [16] Y. Huang, G. Li, C. Chen, Y. Bian, T. Qian, and Z. Bie, "Resilient distribution networks by microgrid formation using deep reinforcement learning," *IEEE Trans. Smart Grid*, vol. 13, no. 6, pp. 4918–4930, Nov. 2022.
- [17] Y. Zhou et al., "Quantum computing in power systems," *iEnergy*, vol. 1, no. 2, pp. 170–187, Jun. 2022.
- [18] N. Nikmehr, P. Zhang, and M. A. Bragin, "Quantum distributed unit commitment: An application in microgrids," *IEEE Trans. Power Syst.*, vol. 37, no. 5, pp. 3592–3603, Sep. 2022.
- [19] N. Nikmehr, P. Zhang, and M. Bragin, "Quantum-enabled distributed unit commitment," in *Proc. IEEE Power Energy Soc. Gen. Meeting*, 2022, pp. 1–5.
- [20] F. Feng, P. Zhang, M. A. Bragin, and Y. Zhou, "Novel resolution of unit commitment problems through quantum surrogate Lagrangian relaxation," *IEEE Trans. Power Syst.*, vol. 38, no. 3, pp. 2460–2471, May 2023.
- [21] J. Gambetta, "IBM's roadmap for scaling quantum technology," 2020. [Online]. Available: <https://research.ibm.com/blog/ibm-quantum-roadmap>
- [22] T. Kadowaki and H. Nishimori, "Quantum annealing in the transverse Ising model," *Phys. Rev. E*, vol. 58, no. 5, 1998, Art. no. 5355.
- [23] S. Tan, J.-X. Xu, and S. K. Panda, "Optimization of distribution network incorporating distributed generators: An integrated approach," *IEEE Trans. Power Syst.*, vol. 28, no. 3, pp. 2421–2432, Aug. 2013.
- [24] H.-G. Yeh, D. F. Gayme, and S. H. Low, "Adaptive VAR control for distribution circuits with photovoltaic generators," *IEEE Trans. Power Syst.*, vol. 27, no. 3, pp. 1656–1663, Aug. 2012.
- [25] Z. Wang, H. Chen, J. Wang, and M. Begovic, "Inverter-less hybrid Voltage/VAR control for distribution circuits with photovoltaic generators," *IEEE Trans. Smart Grid*, vol. 5, no. 6, pp. 2718–2728, Nov. 2014.
- [26] E. Farhi, J. Goldstone, S. Gutmann, and M. Sipser, "Quantum computation by adiabatic evolution," 2000, *arXiv:quant-ph/0001106*.
- [27] S. Boixo et al., "Evidence for quantum annealing with more than one hundred qubits," *Nature Phys.*, vol. 10, no. 3, pp. 218–224, 2014.
- [28] T. Albash and D. A. Lidar, "Adiabatic quantum computation," *Rev. Modern Phys.*, vol. 90, no. 1, 2018, Art. no. 015002.
- [29] A. Lucas, "Ising formulations of many np problems," *Front. Phys.*, vol. 2, 2014, Art. no. 5.
- [30] M. H. Amin, "Consistency of the adiabatic theorem," *Phys. Rev. Lett.*, vol. 102, no. 22, 2009, Art. no. 220401.
- [31] S. Jansen, M.-B. Ruskai, and R. Seiler, "Bounds for the adiabatic approximation with applications to quantum computation," *J. Math. Phys.*, vol. 48, no. 10, 2007, Art. no. 102111.
- [32] E. Farhi, J. Goldstone, S. Gutmann, J. Lapan, A. Lundgren, and D. Preda, "A quantum adiabatic evolution algorithm applied to random instances of an NP-complete problem," *Science*, vol. 292, no. 5516, pp. 472–475, 2001.
- [33] S. Boixo, T. Albash, F. M. Spedalieri, N. Chancellor, and D. A. Lidar, "Experimental signature of programmable quantum annealing," *Nature Commun.*, vol. 4, no. 1, pp. 1–8, 2013.
- [34] C. McGeoch and P. Farré, "The D-Wave advantage system: An overview," D-Wave Syst. Inc., Burnaby, BC, Canada, Tech. Rep. 14-1049A-A, 2020.
- [35] W. H. Kersting, "Radial distribution test feeders," *IEEE Trans. Power Syst.*, vol. 6, no. 3, pp. 975–985, Aug. 1991.
- [36] F. Bu, K. Dehghanpour, Y. Yuan, Z. Wang, and Y. Zhang, "A data-driven game-theoretic approach for behind-the-meter PV generation disaggregation," *IEEE Trans. Power Syst.*, vol. 35, no. 4, pp. 3133–3144, Jul. 2020.



Nima Nikmehr (Senior Member, IEEE) received the Ph.D. degree in electrical engineering from Stony Brook University, Stony Brook, NY, USA, in 2023. He is currently a Project Engineering Senior Professional with Hitachi Energy and a support engineer for NYISO engagement in Albany, NY. His research interests include power system operation and optimization, distribution system resilience, networked microgrids, and quantum computing.

Dr. Nikmehr was the recipient of the Best Paper Award at the 2022 IEEE Power and Energy Society General Meeting for his research on quantum distributed unit commitment. He was also the recipient of the Outstanding Reviewer Award for IEEE Transactions on Sustainable Energy in 2021.



Peng Zhang received the Ph.D. degree in electrical engineering from the University of British Columbia, Vancouver, BC, Canada, in 2009. He is currently a Full Professor of Electrical and Computer Engineering, and a SUNY Empire Innovation Professor with Stony Brook University, Stony Brook, NY, USA. He was a Centennial Associate Professor and a Francis L. Castleman Associate Professor with the University of Connecticut, Storrs, CT, USA. He was a System Planning Engineer at BC Hydro and Power Authority, Canada, during 2006–2010. His research interests include

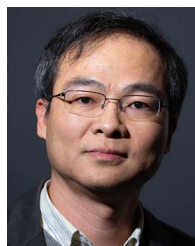
AI-enabled smart grids, quantum-engineered power grids, networked microgrids, power system stability and control, cybersecurity, and formal methods and reachability analysis. His team's pioneering works in quantum computing for power systems won Best Paper Awards at the IEEE Power and Energy Society General Meetings in 2022 and 2020.

Dr. Zhang is an individual member of CIGRÉ. He serves on the editorial boards of several IEEE publications and is the Editor of the IEEE Series on Offshore Wind Energy Collection. He was a 2024 Outstanding Associate Editor for IEEE TRANSACTIONS ON POWER SYSTEMS.



Honghao Zheng (Senior Member, IEEE) received the Ph.D. degree in electrical engineering from the University of Wisconsin-Madison, Madison, WI, USA, in 2015. He is currently the Manager of Market and Operations Analytics with Midcontinent Independent System Operator (MISO), who helps advance business intelligence and data analytics across Market Operations and System Operations by transforming data, increasing understanding and improving visibility into overall market and operations performance and outcomes. Honghao has extensive en-

ergy industry experience, spanning from transmission/distribution operations, technology innovations, software engineering and advanced data analytics. Prior to joining MISO, Honghao was the Manager of Grid Strategy & Analytics in Smart Grid Emerging Technology at Commonwealth Edison, where he led new technology ideation, applied industrial R&D, grid strategy making and complex project execution. Before joining ComEd, he was the tech team lead of Spectrum Power Operator Training Simulator and Transmission Network Applications modules for Siemens Industry. He is a registered Professional Engineer.



Tzu-Chieh Wei received the Ph.D. degree in physics from the University of Illinois, Champaign, IL, USA, in 2004. He is currently a Professor with the C.N. Yang Institute for Theoretical Physics, Stony Brook University, Stony Brook, NY, USA. He was with the interdisciplinary quantum information science and has contributed to the development of the geometric measure of entanglement, quantum computational universality of two-dimensional Affleck-Kennedy-Lieb-Tasaki (AKLT) states, the existence of a nonzero spectral gap in AKLT models, the use of

symmetry-protected topological states for measurement-based quantum computation, QMA-hardness complexity for bosonic problems, and applications of tensor-network methods in quantum many-body systems. He has also involved with several milestone experiments in quantum information processing. His research interests include error mitigation for near-term quantum processors, quantum algorithms, quantum simulations, distributed quantum information processing, and applications of quantum computing. He has spearheaded the effort that led to the creation of a quantum master's program at Stony Brook University, and has been collaborating with colleagues in quantum education for students and teachers.



Gang He received B.S. and M.A. degrees in geography from Peking University, Beijing, China, in 2003 and 2006, respectively, the M.A. degree in climate and society from Columbia University, New York, NY, USA, in 2008, and the Ph.D. degree in energy and resources from the University of California at Berkeley, Berkeley, CA, USA, in 2015. He is currently an Assistant Professor with Baruch College, City University of New York, New York. His research interests include energy systems, energy and climate policy, and energy transition.



Yacov A. Shamash (Fellow, IEEE) received the Ph.D. degree in electrical engineering from the Imperial College of Sciences and Technology, London, U.K. He is currently a Professor of electrical and computer engineering with Stony Brook University, Stony Brook, NY, USA, where he was the Founder of the New York State Center for Excellence in Wireless and in Information Technology, and the New York State Center for Excellence in Advanced Energy Research and Technology. He was the Vice President for Economic Development, Dean of Engineering and Applied Sciences and Harriman School for Management and Policy. He developed and directed the National Science Foundation Industry/University Cooperative Research Center for the Design of Analog/Digital Integrated Circuits and was the Chairman of the Electrical and Computer Engineering Department, Washington State University, Pullman, WA, USA. He serves on the Board of Directors of Comtech Telecommunications Corp., KeyTronic Corp., and Applied DNA Sciences, Inc.

He was the Vice President for Economic Development, Dean of Engineering and Applied Sciences and Harriman School for Management and Policy. He developed and directed the National Science Foundation Industry/University Cooperative Research Center for the Design of Analog/Digital Integrated Circuits and was the Chairman of the Electrical and Computer Engineering Department, Washington State University, Pullman, WA, USA. He serves on the Board of Directors of Comtech Telecommunications Corp., KeyTronic Corp., and Applied DNA Sciences, Inc.